HHS Public Access

Author manuscript

Nature. Author manuscript; available in PMC 2018 August 28.

Published in final edited form as:

Nature. 2018 March 15; 555(7696): 328–333. doi:10.1038/nature25755.

The atomic structure of a eukaryotic oligosaccharyl transferase complex

Lin Bai[1], **Tong Wang**[2], **Gongpu Zhao**[3], **Amanda Kovach**[1], and **Huilin Li**[1,*]

[1]Center for Epigenetics, Van Andel Research Institute, Grand Rapids, Michigan, USA

[2]Advanced Science Research Center at the Graduate Center of the City University of New York, New York, New York, USA

[3]David Van Andel Advanced Cryo-Electron Microscopy Suite, Van Andel Research Institute, Grand Rapids, Michigan, USA

SUMMARY

N-glycosylation is a ubiquitous modification of eukaryotic secretory and membrane-bound proteins; about 90% of glycoproteins are N-glycosylated. The reaction is catalyzed by an eight-protein oligosaccharyltransferase complex, OST, embedded in the ER membrane. Our understanding of eukaryotic protein N-glycosylation has been limited due to the lack of high-resolution structures. Here we report a 3.5-Å resolution cryo-EM structure of the *Saccharomyces cerevisiae* OST, revealing the structures of Ost1–5, Stt3, Wbp1, and Swp1. We found that seven phospholipids mediate many of the inter-subunit interactions, and an Stt3 *N*-glycan mediates interaction with Wbp1 and Swp1 in the lumen. Ost3 was found to mediate the OST-Sec61 translocon interface, funneling the acceptor peptide towards the OST catalytic site as the nascent peptide emerges from the translocon. The structure provides novel insights into co-translational protein N-glycosylation and may facilitate the development of small-molecule inhibitors targeting this process.

INTRODUCTION

N-glycosylation is a predominant modification of proteins in eukaryotic organisms [1–3]. N-linked glycans serve many essential functions, affecting protein folding and sorting in the endoplasmic reticulum (ER) and mediating interactions of the cell or organism with its environment [4]. Proteins are N-glycosylated in the ER lumen by the oligosaccharyltransferase complex (OST), which transfers a pre-formed 14-sugar oligosaccharide from a dolichol-

*Corresponding author: Huilin.Li@vai.org.
Correspondence and requests for materials should be addressed to Huilin.Li@vai.org.

Supplementary Information is available in the online version of the paper.

Author Contributions L.B. and H.L. designed the project. L.B. and A.K. purified proteins. L.B., T.W., and G.Z. collected cryo-EM data. L.B. processed data. L.B. and H.L. analyzed the data and wrote the manuscript.

The authors declare no competing financial interests.

linked donor to selected asparagine residues within a conserved sequon, NXS/T (where X can be any amino acid but proline) [5,6]. Almost two-third of proteins include the NXS/T sequon and 65–75% of them are glycoproteins [4,7]. Mutations in the OST proteins cause a family of diseases known as congenital disorders of glycosylation [8].

The prokaryotic OST is a single-subunit enzyme that is homologous to the eukaryotic catalytic subunit Stt3 [9]. The structures of the bacterial PglB and the archaeal AglB provided first insights into the glycosyl transfer reaction [10–13]. However, prokaryotic protein N-glycosylation is simpler and occurs post-translationally. In contrast, most N-glycosylation in eukaryotes is co-translational [14]. Eukaryotes have evolved a sophisticated machinery to cope with this complexity. *Saccharomyces cerevisiae* has two OST isoforms each with eight membrane proteins: the isoforms contain either Ost3 or Ost6 plus seven shared components: Ost1, 2, 4, and 5; Stt3; Wbp1; and Swp1 [15]. All these subunits have homologs in the metazoan OST [2]: ribophorin I corresponds to the yeast Ost1, DAD1 to Ost2, N33/MagT1 or DC2/KCP2 to Ost3/6, OST4 to Ost4, TMEM258 to Ost5, OST48 to Wbp1, STT3A/STT3B to Stt3, and ribophorin II to Swp1 [16]. Crystal structures of the Ost6 lumenal domain revealed a thioredoxin fold (TRX) [17,18]. The structures of Ost4 were solved by NMR [19,20]. Biochemical studies suggested that Ost1 and Wbp1 recognize acceptor and donor substrates, respectively [8,21,22]. The structures of the eukaryotic OST have been limited to low-resolution EM reconstructions, hindering a mechanistic understanding of protein N-glycosylation in eukaryotes [23–26].

Overall architecture of the OST

OST was purified from yeast strain LY510 (**Online method**). Purified OST is mainly of isoform Ost3, as Ost6 was barely detectable (Extended Data Fig. 1). We determined a 3.5-Å-resolution cryo-EM 3D map and built an atomic model (Fig. 1a–c, Extended Data Figs. 2–3, Extended Data Table 1, Supplementary Videos 1–2). The model contains 4 out of the 5 lumenal domains, 26 out of the 28 TMHs, three *N*-glycans at Asn336 of Ost1p, Asn60 of Wbp1p, and Asn539 of Stt3p, and eight phospholipids.

All five OST soluble domains are in the ER lumen (Fig. 1b–c). The four well-resolved soluble domains are from Stt3, Ost1, Wbp1 and Swp1. The fifth domain is from Ost3, which has TRX activity and interacts with the nascent peptide [17]. This domain is visible in one 3D class, indicating flexibility likely due to the absence of the acceptor peptide (Extended Data Fig. 4). These domains are arranged in an intermediate layer proximal to the membrane and a top layer distal to the membrane. In the intermediate layer, the lumenal domain of Stt3 binds tightly with the middle domain (MD) of Wbp1 and NTD2 of Ost1. In contrast, the three domains in the top layer, NTD of Wbp1, NTD1 of Ost1, and NTD of Swp1, are packed loosely.

Strikingly, the transmembrane domain of OST has a triangular shape in which Stt3 is in the center, surrounded by all other subunits (Extended Data Fig. 5a–c). TMH2-4 of Ost3 pack against TMH10-11 and TMH13 of Stt3, forming the top angle. At the lower right angle, TMH1-3 of Ost2 directly interacts with TMH5 and TMH7-8 of Stt3, and TMH1 of Wbp1 and TMH1-3 of Swp1 are further out, interacting with Ost2. TMH1 of Ost1 and TMH1-2 of Ost5 are loosely organized and constitute the lower left angle. The two missing TMHs,

TMH9 of Stt3 and TMH1 of Ost3, surround the lipid-linked oligosaccharide (LLO) docking site and are presumably flexible in the absence of the donor.

The structure of Stt3

The catalytic subunit Stt3 comprises 13 TMHs, a lumenal domain, and an α-helical accessory domain that is formed by external loop 1 (EL1) (Fig. 2a–b). The 13-TMH topology is consistent with a recent characterization of yeast and mouse Stt3 and is similar to the prokaryotic homologues [13,27]. The Stt3 lumenal domain is a mixed α/β fold, similar to the prokaryotic counterparts [10–13,28], but it is different from the NMR structure of the yeast Stt3 that was derived from proteins refolded in the presence of the denaturing sodium dodecyl sulfate [29]. The structural conservation between Stt3 and prokaryotic enzymes is remarkable, considering their ~20% sequence identity. The bacterial enzymes have an extended acceptor sequon of DXNXS/T [30]. The −2 position D is stabilized by R331 in the PglB crystal structure [13]. PglB R331 is replaced by D362 in yeast Stt3, explaining the shorter eukaryotic sequon of NXS/T. Notably, the yeast Stt3 has a carboxyl terminal extension (CTE) that mediates the interaction between Wbp1 and Swp1 (Fig. 2a, 2c, Extended Data Fig. 3). The Stt3 CTE is apparently a eukaryote-specific feature as it is absent in prokaryotes (Extended Data Figs. 6–7). The CTE of the metazoan STT3A is shorter than that of the STT3B. It would be interesting to investigate whether the longer CTE endows the STT3B isoform with the capacity to post-translationally glycosylate the extreme C-terminal acceptor sites of the nascent polypeptides that have been skipped by the STT3A isoform [31].

There is a horizontal substrate-binding groove in Stt3 between the transmembrane domain and lumenal domain. The roof of the groove is lined by the highly conserved glycosylation-sequon-binding WWD motif. Compared with the periplasmic domain of PglB in complex with a peptide substrate, the Stt3 lumenal domain is shifted outwards by 3 Å, leading to a widened groove (Fig. 2b), which may facilitate substrate binding. Relative to PglB, TMH1 and TMH13 in Stt3 move away from each other to accommodate the sole TMH of Ost4; in this regard, Ost4 may be considered as an integral part of Stt3 (Extended Data Fig. 5c). TMH8-9 slide by 25 Å toward the LLO-binding surface, leaving a space for Ost2 TMH1-2. Stt3 residues that are expected to coordinate Mn^{2+} and LLO, such as D47, D166, E168, W208, and R404, are superimposable with their respective counterparts in PglB (Extended Data Fig. 6, Fig. 2b).

The Stt3 *N*-glycan in the N539-N540-T541 sequon interacts with D320, Y322 and R349 of Wbp1 and with H182 in the linker loop of Swp1(Fig. 2a, 2d), suggesting that the glycan stabilizes the complex by gluing these subunits together. A previous study showed that N539Q mutation is lethal, and T541A mutation is severely temperature-sensitive [32].

Ordered phospholipids mediate OST assembly

The eight OST subunits can be grouped into three subcomplexes: Ost1–Ost5, Ost2–Swp1–Wbp1, and Stt3–Ost3–Ost4 (Fig. 3a–b). This architecture is consistent with a previous crosslinking studies [33]. The interfaces among the three subcomplexes in the membrane region are loose, with only a few protein-protein interactions between Ost2 and Stt3. We

identified seven phospholipids (PL1–7) at the interfaces of these subcomplexes, and an eighth phospholipid (PL8) at the donor binding site in Stt3, to be described below; each of these lipid molecules has well-defined electron densities (Extended Data Fig. 3, Fig. 3c–d). PL1–3 fill a 15-Å gap at the interface between Stt3 and Ost1-Ost5. Their hydrophilic groups interact with W241, Q250, E252, D301, Y303, and Y409 of Ost1, R112 and N113 of Stt3, and Y85 of Ost5. The lipid tails contact hydrophobic residues in TMH1-2 of Stt3 and TMH2 of Ost5 (Fig. 3c). PL4–5 mediate the interaction between Stt3 and Ost2-Swp1 (Fig. 3d). Their tails interact with hydrophobic residues of TMH3 of Ost2, TMH2-3 of Swp1, TMH5 and EL1 of Stt3, whereas the phosphate groups directly hydrogen-bond to the side chains of N380, D381, and R385 of Wbp1. PL6–7 stabilize the interface of Stt3 and Ost2-Swp1. Many of these phospholipid-interacting residues are conserved (Extended Data Figs. 7–9). Lipids are known to play important roles in membrane enzyme complexes [34,35] and can mediate transient multimerization of membrane proteins [36]. A recent cryo-EM structure showed that lipids are involved in the assembly of the heterotetrameric γ-secretase [37].

Structures of the noncatalytic subunits

In the Ost1–Ost5 subcomplex, the Ost1 contains two lumenal domains, NTD1 and NTD2; both are composed of a larger seven-stranded β-sheet with a smaller, four-stranded β-sheet attached at each end, and on the same face of, the larger sheet. NTD1 and NTD2 are superimposable with a root-mean-square-deviation (rmsd) of 2.8 Å, despite their 9% sequence identity (Fig. 4a–b). This fold is similar to the noncatalytic domain of leukotriene A-4 aminopeptidase (rmsd 2.9 Å). Because Ost1 can bind the glycosylated, but not the unglycosylated, sequon [22], NTD1 and NTD2 may function to prevent the glycosylated peptide from sliding back to the catalytic site. Perhaps related to this function, the Ost1 NTD2 has an extra conserved hydrophobic motif (relative to NTD1) that specifically binds to the Stt3 catalytic domain (Fig. 4b, Extended Data Fig. 8). Ost5 appears to be an accessary factor of Ost1, as its two TMHs pack against the sole TMH of Ost1, and the N-terminal lumenal 20 residues of Ost5 latches onto the Ost1 NTD2, positioning Ost1 NTD2 for interaction with Stt3 (Figs. 3 and 4).

The Ost2–Swp1–Wbp1 subcomplex contains three soluble domains: the NTD and MD of Wbp1 and NTD of Swp1 (Fig. 4c). The NTD and linker loop of Swp1 interact extensively with the NTD and MD of Wbp1. In the membrane region, four TMHs of Ost2 and three TMHs of Swp1 surround the sole TMH of Wbp1 (Fig. 4c). The functions of these domains are largely unknown, except that Wbp1 contains a GIFT domain (for the bacterial gliding protein GldD, intraflagellar transport [IFT]) and therefore may be involved in LLO binding [38]. The Wbp1 NTD is superimposable with the NTD of IFT52 (Fig. 4d; rmsd 2.9 Å), and that the MD of Wbp1 is similar to amylase domain N (Fig. 4e; rmsd 2.7 Å), which has a pullulan binding site. The Swp1 NTD resembles the MD-1, a lipopolysaccharide (LPS)- and sugar-binding co-receptor of the RP105-MD-1 Toll-like receptor complex (Fig. 4f; rmsd 3.5 Å). These results suggest that both Wbp1 and Swp1 are involved in recruiting LLO. Indeed, Wbp1 and its mammalian homolog OST48 were shown to crosslink with LLO [21,39].

In the Stt3–Ost4–Ost3 subcomplex, Ost4 stabilizes the Stt3 structure (Extended Data Fig. 5a–b). Ost3 has three TMHs that interact with TMH10, 11, and 13 of Stt3. Interestingly,

TMH2 of Ost3 and TMH6 and TMH11 of Stt3 form a vertical groove that may function as LLO docking site (Fig. 5a–b). Consistent with this possibility, W208 at the upper half of the groove, close to the catalytic center (Figs. 2b, 5c), was previously shown to be lethal when mutated to alanine in Stt3 [40]. The corresponding W215A mutation in AglB reduced the activity [11], and the PglB equivalent Y196 directly interact with LLO [12]. The lower half of this groove is lined with numerous hydrophobic residues and is occupied by phospholipid PL8 in our structure (Fig. 5c). Superposition of the structure of the PglB bound to the acceptor peptide and donor analog with the Stt3 structure showed that the acceptor fits right into the putative active site and LLO analog fits in potential LLO-docking vertical groove in Stt3 (Figs. 2b, 5c).

The LLO entry route and lateral helix of Ost2

The EL5 loop of PglB is disordered in the absence of the donor, but becomes ordered when both donor and acceptor substrates are present [12,13,41] (Fig. 5d). It was proposed that EL5 disordering allows the donor to diffuse under it into the catalytic site [12]. Eukaryotic LLO is much larger, both in the dolichol-binding transmembrane region and the OS-binding lumenal region: the yeast dolichol contains 14–18 repeating isoprene units, twice that of bacterial LLO [42], and the yeast OS contains 14 sugars compared with the 7-sugar bacterial OS. As such, the donor docking and recognition mechanisms of these two enzymes are likely different. Indeed, as described above, there is a large membrane-embedded pocket inside OST formed by TMH2 of Ost3 and TMH6, TMH8, and TMH11 of Stt3 (Fig. 5a–b). The disordered EL5 and TMH9 of Stt3 and TMH1 of Ost3 enlarge the donor-binding pocket. Further, the Stt3 TMHs 8 and 9 slide towards the LLO-binding surface by about 25 Å relative to that of PglB (as described above) and form a lumenally unobstructed 10-Å-wide gap. The yeast OS is likely too large to dive under the disordered EL5 to enter the catalytic site. We suggest that yeast LLO enters the catalytic site via the 10-Å gap between TMH8 and TMH9 in Stt3. This route has the added advantage of being closer to Wbp1 and Swp1, the potential LLO recruiters (Fig. 5a–b). Consistent with two distinct LLO access routes between OST and PglB, the PglB TMH8 and TMH9 are far from the LLO binding site, tightly packed against other TMHs, and do not change their location whether the LLO is present or not (Fig. 5d, Extended Data Fig. 5c).

Ost2 has a cytoplasmic lateral α-helix (LH) (Fig. 1c, Fig. 5a–b). The LH stabilizes Stt3 TMH8-9 hairpin, and interacts with Swp1 TMH3 and WBP1 TMH1, both of which extend towards their respective lumenal domains. Because Stt3 TMH9 is largely disordered in the absence of donor, binding of dolichol will likely cause ordering of TMH9, which may be sensed by and communicated through the LH to the lumenal domains of Swp1 and Wbp1 via their respective TMH3 and TMH1. Because Swp1 and Wbp1 are involved in OS binding, such a relay mechanism via the LH may lead to coordination between the binding of dolichol in the membrane and OS binding in the lumen.

Ost3 mediates the OST/translocon interface

OST and the Sec61 complex simultaneously bind to ribosomes in vitro [43]. Recent cryo-electron tomographic studies showed the relative positions of mammalian translocons and OSTs bound to the ribosomes [24,26]. However, the detailed interface—i.e., which subunits

mediate the OST/translocon interaction—was unclear. We docked the yeast OST atomic model into the cryo-electron tomogram and found that it fit well into the mammalian OST density except for two extra densities (Fig. 6a). These densities likely belong to the NTD of mammalian ribophorin II and CTD of ribophorin I, because only ribophorin I and II contain the extra sizable sequences (Extended Data Figs. 8–9). We further docked the crystal structure of a mammalian Sec61 into the tomogram and identified Ost3 as mediating the OST interaction with the translocon (Supplementary Video 3). Specifically, the Ost3 TMH3-4 pack tightly with TMH1 of Sec61α, TMH2 of Sec61β, and the sole TMH of Sec61γ (Fig. 6b). This finding explains why the two yeast OST isoforms are defined by the presence of either Ost3 or Ost6: they interact with the Sec61 and Ssh1 translocons, respectively [15]. Our finding is also in agreement with the finding that that DC2 and KCP2 mediate the interaction between the human OST and translocon [44].

Based on these observations, we proposed a pathway for the nascent peptide during the co-translational N-glycosylation (Fig. 6b). Specifically, the nascent peptide emerging from the Sec61 translocon is first captured by the lumenal TRX of Ost3 and then is threaded through the Stt3 catalytic site for N-glycosylation. Finally, the glycosylated peptide is stabilized by the two lumenal domains of Ost1, perhaps to prevent its backtracking.

Conclusion

Our cryo-EM study of the eukaryotic OST provides the atomic models of all eight component membrane proteins, reveals how these subunits assemble into a functional complex, and suggests functions for many of the subunits. Given the critical role of protein N-glycosylation in tumorigenesis and diagnosis [45,46], the structure may serve as a platform for the development of small-molecule inhibitors targeting the N-glycosylation-related diseases in humans.

METHODS

Purification of the OST Complex

The OST complex was purified from the yeast strain LY500 as previously described [23]. Briefly, cells were lysed by French press at 15,000 psi, and microsomes were collected by centrifugation. The membrane pellet was then resuspended and dissolved in buffer containing 10% glycerol, 20 mM Tris-HCl (pH 7.4), 1.5% digitonin, 0.5 M NaCl, 1 Mm $MgCl_2$, 1 mM $MnCl_2$, 1 mM EDTA, and 1 mM phenylmethylsulfonyl fluoride. After incubation for 30 min, the mixture was centrifuged for 30 min at 120,000 × *g*, and the clarified supernatant was mixed with pre-washed anti-FLAG (M2) affinity gel at 4 °C overnight with shaking. The affinity gel was collected by centrifugation and washed three times in buffer A containing 0.2% digitonin, 150 mM NaCl, 20 mM Tris-HCl (pH 7.4), 1 mM $MgCl_2$, 1 mM $MnCl_2$. Finally, the OST was eluted with buffer A containing 0.15 mg/ml 3X FLAG peptide, and further purified in a Superose 6 10/300 gel filtration column in buffer A. The quality of the final sample was confirmed by SDS-PAGE gel. To examine the presence of Ost3/Ost6 in the purified complex, three bands around 30 kD in the SDS-PAGE were cut out and identified by tryptic digestion and mass spectrometry.

Cryo-electron microscopy

Aliquots of 3 μl of purified OST at a concentration of 5 mg/ml were placed on glow-discharged holey carbon grids (Quantifoil Au R1.2/1.3, 300 mesh) and flash-frozen in liquid ethane using an FEI Vitrobot Mark IV. The grids were then loaded into an FEI Titan Krios electron microscope operated at a high tension of 300 kV and images were collected automatically with EPU (FEI) at a nominal magnification of 130,000× in EFTEM mode and a pixel size of 1.088 Å per pixel with defocus values from −1.5 to −2.5 μm. A Gatan K2 Summit direct electron detector was used under super resolution counting mode for image recording. A BioQuantum energy filter installed in front of the K2 detector was operated in zero-energy-loss mode with an energy slit width of 20 eV. The dose rate was 10 electrons per $Å^2$ per second, and the total exposure time was 6 s. The total dose was divided into a 30-frame movie so each frame was exposed for 0.2 s.

Image processing

About 4,000 raw movie micrographs were collected and motion-corrected using the program MotionCorr 2.0 [47]. Contrast transfer function parameters of each aligned micrograph were calculated using GCTF [48]. All the remaining steps, including particle auto selection, 2D classification, 3D classification, 3D refinement, and density map postprocessing, were performed using RELION 2.0 [49]. Templates for automatic picking were generated from 2D averages of about 10,000 manually picked particles. A total of 823,255 particles were picked automatically. 2D classification was then performed and particles in the classes with features unrecognizable by visual inspection were removed. A total of 369,452 particles was used for further 3D classification, and 282,202 particles were selected for further 3D refinement and postprocessing, resulting in the 3.5-Å 3D density map. The resolution of the map was estimated by the gold-standard Fourier shell correlation at a correlation cutoff value of 0.143.

Structural Modeling, Refinement, and Validation

The initial models of Stt3, the soluble domain of Ost1, and the NTD of Wbp1 were generated, respectively, from the crystal structures of *Archaeoglobus fulgidus* oligosaccharyltransferase (Protein Data Bank (PDB) ID 3WAK), Leukotriene A-4 hydrolase (PDB ID ID 5NI2), and IFT52 (PDB ID ID 5FMS) using the online server SWISSMODEL (https://swissmodel.expasy.org). The model of Stt3 was split into a transmembrane domain and a periplasmic domain. These models were docked into the 3.5-Å EM map in COOT and Chimera [50,51]. All other subunits of OST were manually built into the remaining density in the program COOT. Sequence assignment was guided by bulky residues such as Phe, Tyr, Trp, and Arg. The entire OST model was then refined by rigid-body refinement of individual chains in the PHENIX program and subsequently was adjusted manually in COOT [52]. There were densities for eight lipid molecules, each with well-defined densities for a head group and two tails. However, the precise chemical nature of the head group is unclear due to the limited resolution. We modeled all lipids as a phosphatidylcholine, which is the most common lipid (~60% phospholipid) in the ER membrane. The final model was also cross-validated as described before [53]. Using the PDB tools in Phenix, the coordinates of the final model was firstly randomly added 0.1 Å noise, and then this noise-added model was

performed one round of refinement against the first half-map (Half1) that was produced during 3-D refinement by RELION. We then correlated the refined model with the 3D maps of the two half-maps (Half1 and Half2) to produce two FSC curves: FSC_{work} (Model vs. Half1 map) and FSC_{free} (Model vs. Half2 map). Besides, we generated a third FSC curve using the final model and the final 3.5-Å-resolution density map produced from all particles. The general agreement of these curves was taken as an indication that the model was not over-fitted. Finally, the atomic model was validated using MolProbity [54]. Structural figures were prepared in Chimera and PyMOL (https://pymol.org/2/).

Data Availability

The cryo-EM 3D map of the *S. cerevisiae* OST complex has been deposited at the EMDB database with accession code EMD-7336. The corresponding atomic model was deposited at the RCSB PDB with accession code 6C26.

Extended Data

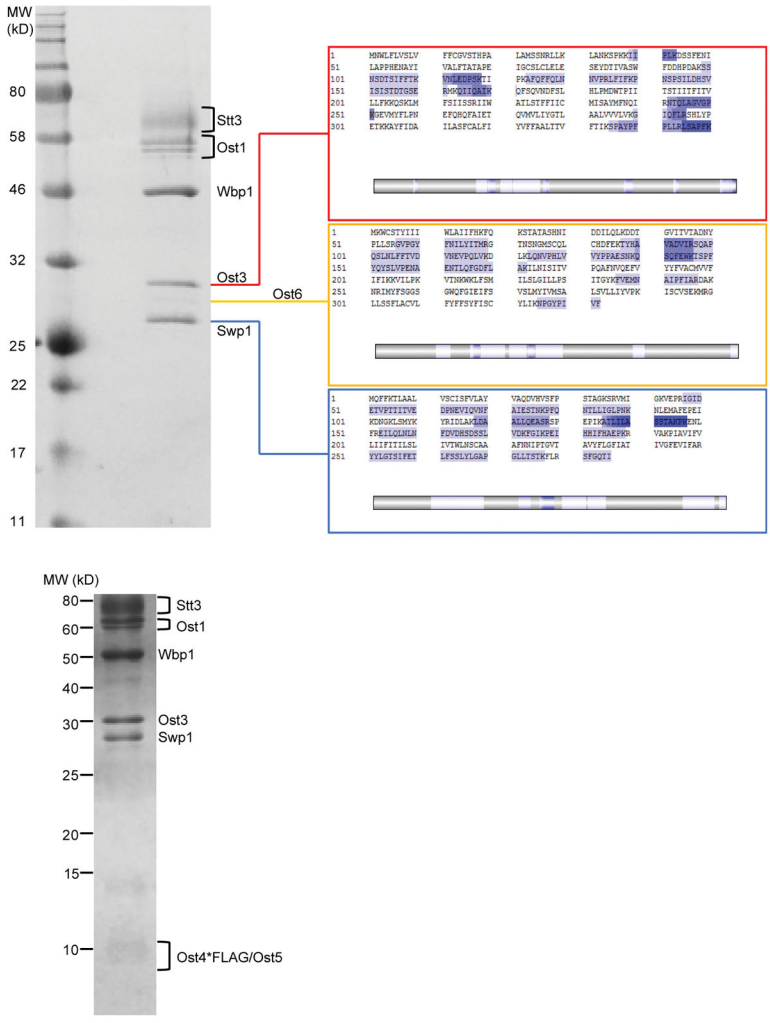

Extended Data Figure 1. Identification of Ost3/Ost6 by mass spectrometry

(a) The Coomassie blue–stained SDS-PAGE gel of the purified OST complex. The small subunits Ost2, Ost4-FLAG, and Ost5 were not visible in this 12% acrylamide SDS-PAGE gel because of their weak density. (**b**) Sequence coverage of tryptic digestion mass spectrometry (MS) of three bands at around 30 kDa that are labeled as Ost3, Ost6, and Swp1. The detected peptides are highlighted in blue. The lower bars under the sequences indicate matched peptides. Darker blue indicates more overlaps of peptides detected. (**c**) Ost2, Ost4-FLAG, and Ost5 were seen in the 15% acrylamide SDS-PAGE gel that was run slower and stained longer. For panel (**a**) and (**c**), the experiments were repeated more than 3 times with similar results.

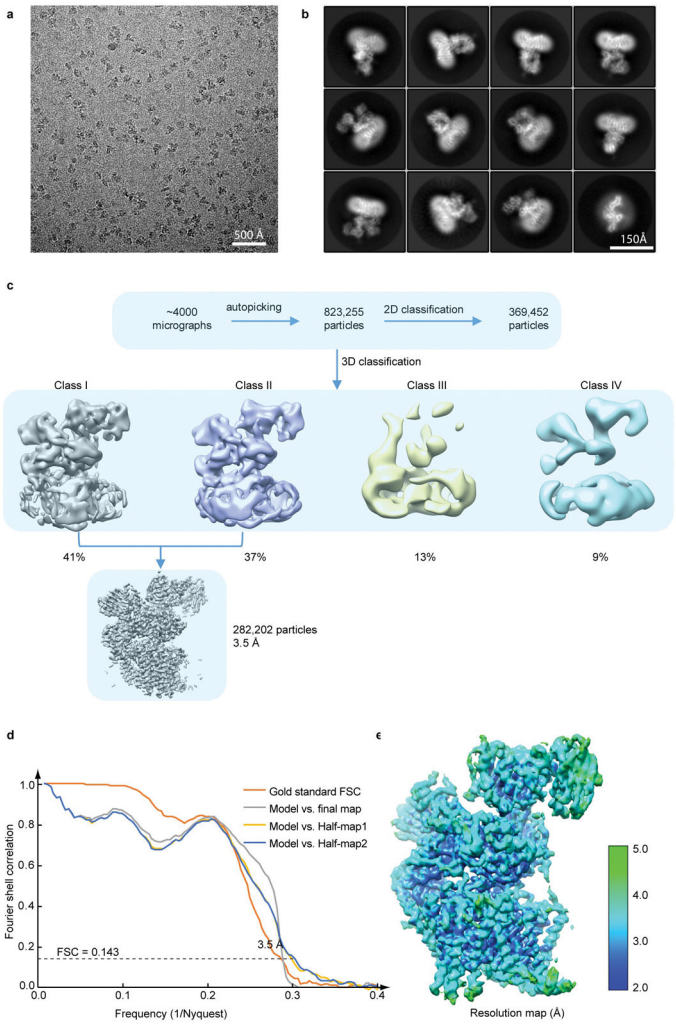

Extended Data Figure 2. Single-particle cryo-EM analysis of the OST complex

(a) A representative electron micrograph of the OST imaged in the Titan Krios with a K2 detector. About 4000 similar micrographs were recorded. (**b)** Selected reference-free 2D class averages. **(c)** 2D and 3D image classification procedure. **(d)** Gold-standard Fourier correlation of two independent half maps, and the validation correlation curves of the atomic model by comparing the model with the final map or with the two half maps. **(e)** Local resolution map of the OST complex structure.

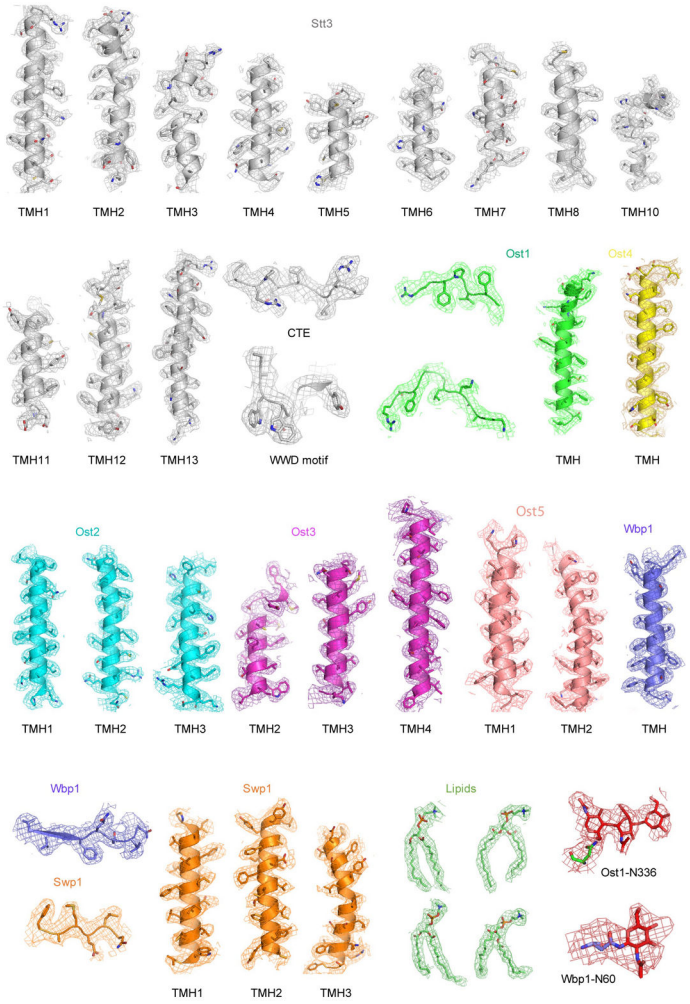

Extended Data Figure 3. A gallery of selected regions in the OST structure, illustrating the fitting between the 3D density map and the atomic model

These include 26 TMHs, several regions in the lumenal domains, four selected lipids, and two *N*-glycans.

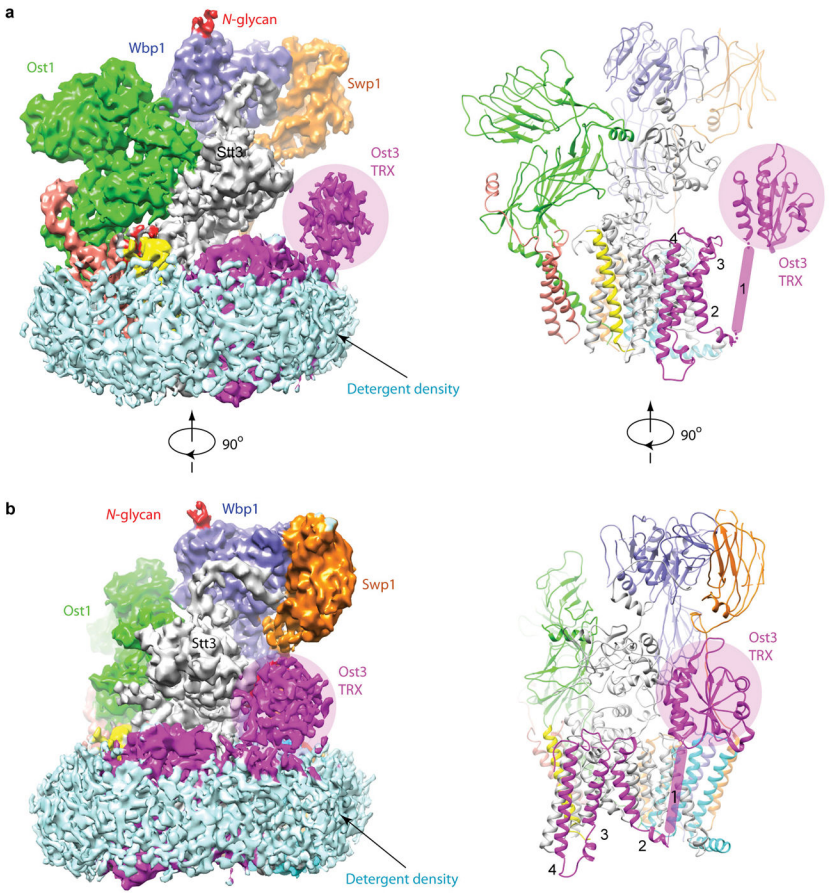

Extended Data Figure 4. EM density map of the TRX domain of Ost3

(**a–b**) From 3D classification, one class (Class I) contained stronger Ost3 TRX domain density than other classes. This map was further refined to 4.4 Å. Surface view of the map (left) and the corresponding cartoon view of the atomic model (right), colored by subunit, are shown in two orthogonal side views. The N-terminal thioredoxin domain (TRX) of Ost3 is highlighted by a magenta disk and is visible in this low-threshold display. The detergent densities surrounding the transmembrane region of OST is visible at this threshold, and are colored in cyan. The structure of the homologous Ost6 TRX (PDB ID 3G7Y) is tentatively placed for the purpose of domain location.

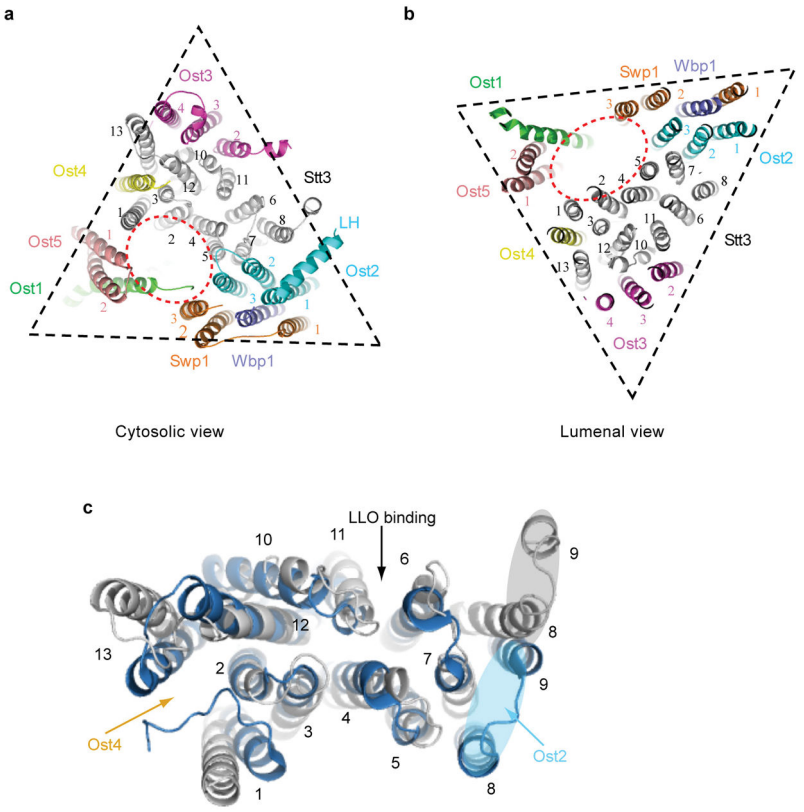

Extended Data Figure 5. The transmembrane region of the OST complex

The TMHs of OST form a triangular shape and shown in cytoplasmic view (**a**) and lumenal view (**b**). The catalytic subunit Stt3 is in the center, surrounded by the other subunits. There is a sizable cavity in the center (red dotted circle). **(c)** Superposition of the transmembrane region of Stt3 and PglB (PDB ID 5OGL) viewed from the cytoplasmic side. The Stt3 TMH8-9 (light gray ellipse) moves towards the LLO biding surface relative to the TMHs8-9 of PglB (light blue ellipse), creating space for the Ost2 TMHs. The Stt3 TMH1 and TMH13 also move apart, forming a space for the only TMH of Ost4.

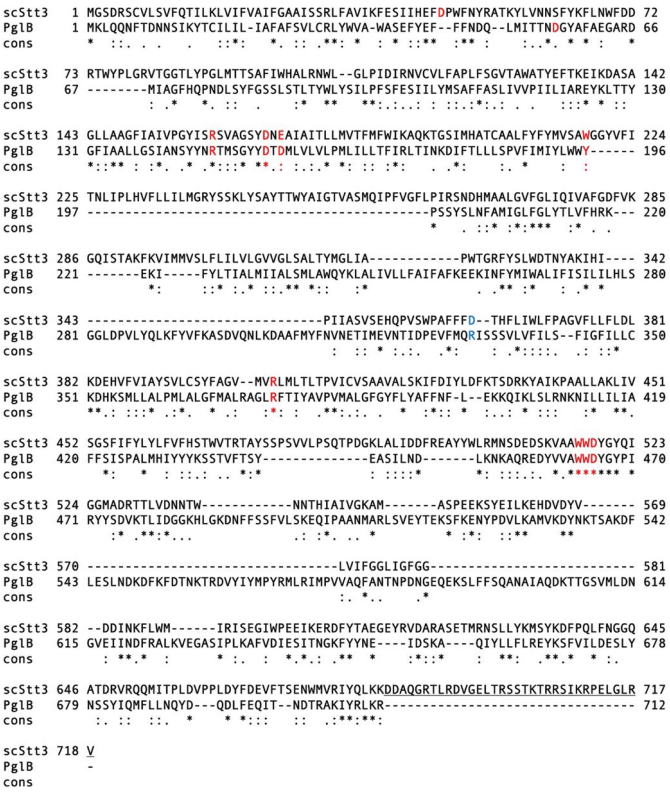

Extended Data Figure 6. Sequence alignments of *S. cerevisiae* Stt3 and *A. fulgidus* PglB

PglB doesn't have the CTE sequence (underscored) found in the yeast Stt3 and human STT3B. Several conserved residues in the active site are highlighted in red. R331 in the PglB, which stabilizes the −2 position D of the acceptor peptide, is highlighted in blue. An asterisk (*) indicates positions with identical residue, a colon (:) indicates strong conservation, and a period (.) indicates weak conservation.

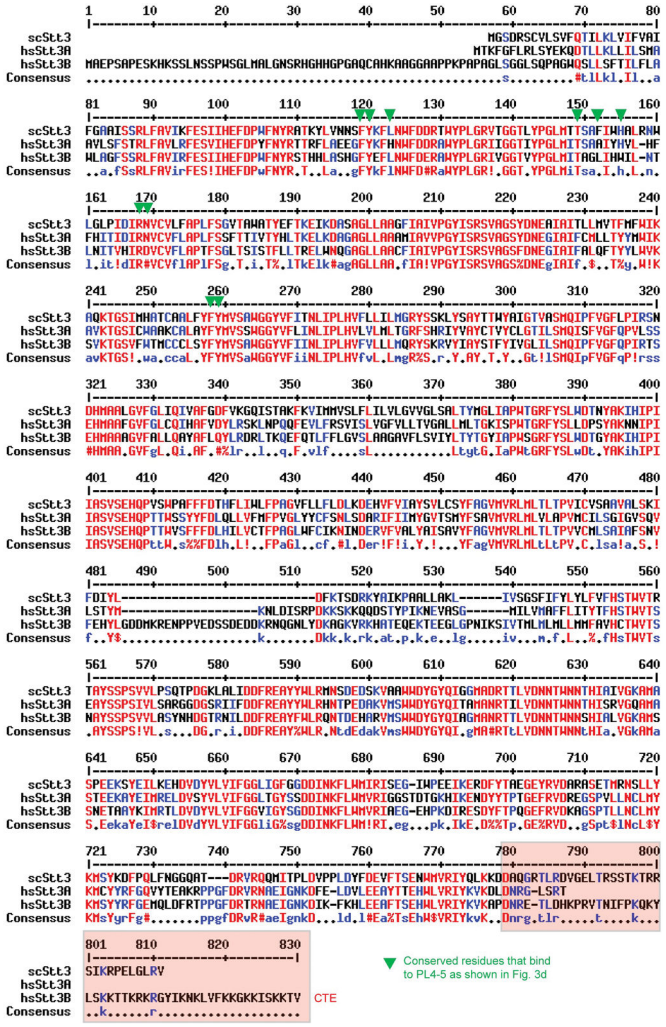

Extended Data Figure 7. Sequence alignment of selected eukaryotic Stt3

sc: *Saccharomyces cerevisiae*, hs: *Homo sapiens*. The CTE of human STT3A is shorter than those of STT3B and yeast Stt3.

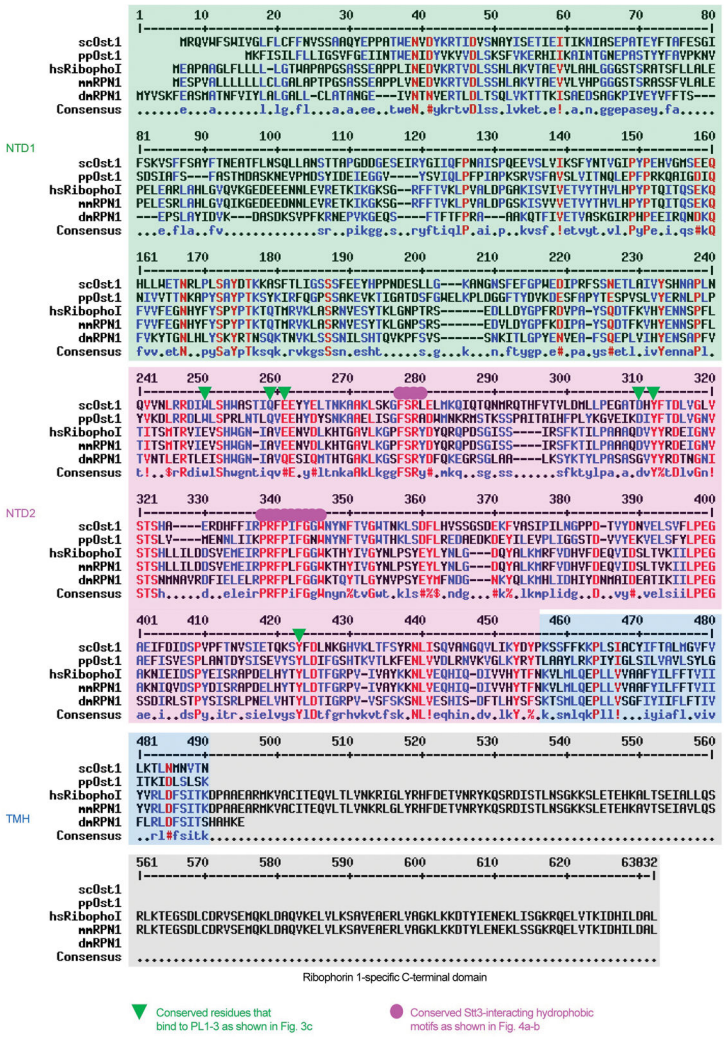

Extended Data Figure 8. Sequence alignment of selected eukaryotic Ost1

sc: *Saccharomyces cerevisiae*, pp: *Pichia pastoris*, hs: *Homo sapiens*, mm: *Mus musculus*, and dm: *Drosophila melanogaster*. An extra CTD in ribophorin I of higher organisms is not present in the yeast proteins (shaded gray). NTD1 is shaded in light green, NTD2 in light magenta, TMH in light blue, and the CTD of ribophorin I of higher organisms in light gray.

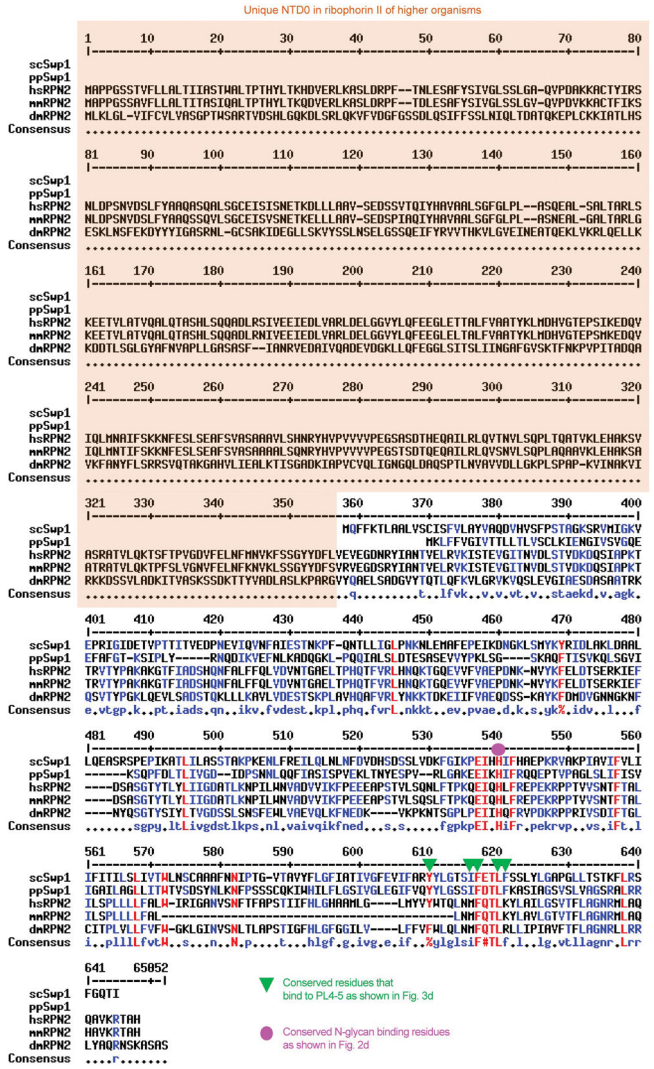

Extended Data Figure 9. Sequence alignment of selected eukaryotic Swp1

sc: *Saccharomyces cerevisiae*, pp: *Pichia pastoris*, hs: *Homo sapiens*, mm: *Mus musculus*, and dm: *Drosophila melanogaster*. Ribophorin II of higher organisms has evolved an extra N terminal domain (NTD0, shaded in light orange) in the lumen that is not present in the two yeast proteins.

Extended Data Table 1

Cryo-EM data collection, refinement and validation statistics.

	***S. cerevisiae* OST complex (EMD-7336) (PDB 6C26)**
Data collection and processing	
Microscope	FEI Titan Krios
Voltage (kV)	300
Electron exposure (e–/Å^2)	60

	***S. cerevisiae* OST complex (EMD-7336) (PDB 6C26)**
Defocus range (μm)	1.5–2.5
Pixel size (Å)	1.088
Symmetry imposed	C1
Initial particle images (no.)	823255
Final particle images (no.)	282202
Map resolution (Å)	3.5
FSC threshold	0.143
Map resolution range (Å)	278.5–3.5
Refinement	
Map sharpening *B* factor ($Å^2$)	144.159
Model composition	
Non-hydrogen atoms	17202
Protein residues	2039
Lipids	8
N-glycans	3
R.m.s. deviations	
Bond lengths (Å)	0.01
Bond angles (°)	1.24
Validation	
MolProbity score	1.89
Clashscore	5.31
Poor rotamers (%)	1.15
Ramachandran plot	
Favored (%)	89.6
Allowed (%)	10.4
Disallowed (%)	0

Supplementary Material

Refer to Web version on PubMed Central for supplementary material.

Acknowledgments

Cryo-EM images were collected in the David Van Andel Advanced Cryo-Electron Microscopy Suite at Van Andel Research Institute. We thank Yoichiro Harada for advice on yeast genetics and David Nadziejka for proofreading. This work was partially supported by Van Andel Research Institute (to H.L.) and the U.S. National Institutes of Health (GM111742 to H.L.).

References

1. Larkin A, Imperiali B. The expanding horizons of asparagine-linked glycosylation. Biochemistry-Us. 2011; 50:4411–4426.
2. Cherepanova N, Shrimal S, Gilmore R. N-linked glycosylation and homeostasis of the endoplasmic reticulum. Curr Opin Cell Biol. 2016; 41:57–65. [PubMed: 27085638]

3. Dempski RE Jr, Imperiali B. Oligosaccharyl transferase: gatekeeper to the secretory pathway. Curr Opin Chem Biol. 2002; 6:844–850. [PubMed: 12470740]
4. Mohorko E, Glockshuber R, Aebi M. Oligosaccharyltransferase: the central enzyme of N-linked protein glycosylation. J Inherit Metab Dis. 2011; 34:869–878. [PubMed: 21614585]
5. Kornfeld R, Kornfeld S. Assembly of asparagine-linked oligosaccharides. Annu Rev Biochem. 1985; 54:631–664. [PubMed: 3896128]
6. Helenius A, Aebi M. Roles of N-linked glycans in the endoplasmic reticulum. Annu Rev Biochem. 2004; 73:1019–1049. [PubMed: 15189166]
7. Apweiler R, Hermjakob H, Sharon N. On the frequency of protein glycosylation, as deduced from analysis of the SWISS-PROT database. Bba-Gen Subjects. 1999; 1473:4–8.
8. Hennet T, Cabalzar J. Congenital disorders of glycosylation: a concise chart of glycocalyx dysfunction. Trends Biochem Sci. 2015; 40:377–384. [PubMed: 25840516]
9. Nothaft H, Szymanski CM. Protein glycosylation in bacteria: sweeter than ever. Nat Rev Microbiol. 2010; 8:765–778. [PubMed: 20948550]
10. Matsumoto S, Taguchi Y, Shimada A, Igura M, Kohda D. Tethering an N-Glycosylation Sequon-Containing Peptide Creates a Catalytically Competent Oligosaccharyltransferase Complex. Biochemistry-Us. 2017; 56:602–611.
11. Matsumoto S, et al. Crystal structures of an archaeal oligosaccharyltransferase provide insights into the catalytic cycle of N-linked protein glycosylation. P Natl Acad Sci USA. 2013; 110:17868–17873.
12. Napiorkowska M, et al. Molecular basis of lipid-linked oligosaccharide recognition and processing by bacterial oligosaccharyltransferase. Nat Struct Mol Biol. 2017
13. Lizak C, Gerber S, Numao S, Aebi M, Locher KP. X-ray structure of a bacterial oligosaccharyltransferase. Nature. 2011; 474:350–355. [PubMed: 21677752]
14. Kelleher DJ, Gilmore R. An evolving view of the eukaryotic oligosaccharyltransferase. Glycobiology. 2006; 16:47R–62R.
15. Yan AX, Lennarz WJ. Two oligosaccharyl transferase complexes exist in yeast and associate with two different translocons. Glycobiology. 2005; 15:1407–1415. [PubMed: 16096345]
16. Shrimal S, Cherepanova NA, Gilmore R. Cotranslational and posttranslocational N-glycosylation of proteins in the endoplasmic reticulum. Semin Cell Dev Biol. 2015; 41:71–78. [PubMed: 25460543]
17. Schulz BL, et al. Oxidoreductase activity of oligosaccharyltransferase subunits Ost3p and Ost6p defines site-specific glycosylation efficiency. P Natl Acad Sci USA. 2009; 106:11061–11066.
18. Mohorko E, et al. Structural Basis of Substrate Specificity of Human Oligosaccharyl Transferase Subunit N33/Tusc3 and Its Role in Regulating Protein N-Glycosylation. Structure. 2014; 22:590–601. [PubMed: 24685145]
19. Gayen S, Kang CB. Solution structure of a human minimembrane protein Ost4, a subunit of the oligosaccharyltransferase complex. Biochem Bioph Res Co. 2011; 409:572–576.
20. Zubkov S, Lennarz WJ, Mohanty S. Structural basis for the function of a minimembrane protein subunit of yeast oligosaccharyltransferase. Proc Natl Acad Sci U S A. 2004; 101:3821–3826. [PubMed: 15001703]
21. Pathak R, Hendrickson TL, Imperiali B. Sulfhydryl Modification of the Yeast Wbp1p Inhibits Oligosaccharyl Transferase-Activity. Biochemistry-Us. 1995; 34:4179–4185.
22. Yan Q, Prestwich GD, Lennarz WJ. The Ost1p subunit of yeast oligosaccharyl transferase recognizes the peptide glycosylation site sequence, -Asn-X-Ser/Thr- J Biol Chem. 1999; 274:5021–5025. [PubMed: 9988747]
23. Li H, Chavan M, Schindelin H, Lennarz WJ, Li HL. Structure of the oligosaccharyl transferase complex at 12 angstrom resolution. Structure. 2008; 16:432–440. [PubMed: 18334218]
24. Pfeffer S, et al. Structure of the native Sec61 protein-conducting channel. Nat Commun. 2015; 6
25. Pfeffer S, et al. Structure of the mammalian oligosaccharyltransferase complex in the native ER protein translocon. Nat Commun. 2014; 5
26. Pfeffer S, et al. Dissecting the molecular organization of the translocon-associated protein complex. Nat Commun. 2017; 8

27. Lara P, et al. Refined topology model of the STT3/Stt3 protein subunit of the oligosaccharyltransferase complex. J Biol Chem. 2017; 292:11349–11360. [PubMed: 28512128]
28. Igura M, et al. Structure-guided identification of a new catalytic motif of oligosaccharyltransferase. EMBO J. 2008; 27:234–243. [PubMed: 18046457]
29. Huang C, Bhaskaran R, Mohanty S. Eukaryotic N-glycosylation occurs via the membrane-anchored C-terminal domain of the Stt3p subunit of oligosaccharyltransferase. J Biol Chem. 2012; 287:32450–32458. [PubMed: 22865878]
30. Kowarik M, et al. Definition of the bacterial N-glycosylation site consensus sequence. EMBO J. 2006; 25:1957–1966. [PubMed: 16619027]
31. Shrimal S, Trueman SF, Gilmore R. Extreme C-terminal sites are posttranslocationally glycosylated by the STT3B isoform of the OST. J Cell Biol. 2013; 201:81–95. [PubMed: 23530066]
32. Li GT, Yan Q, Nita-Lazar A, Haltiwanger RS, Lennarz WJ. Studies on the N-glycosylation of the subunits of oligosaccharyl transferase in Saccharomyces cerevisiae. J Biol Chem. 2005; 280:1864–1871. [PubMed: 15507441]
33. Yan A, Ahmed E, Yan Q, Lennarz WJ. New findings on interactions among the yeast oligosaccharyl transferase subunits using a chemical cross-linker. J Biol Chem. 2003; 278:33078–33087. [PubMed: 12805367]
34. Palsdottir H, Hunte C. Lipids in membrane protein structures. Biochim Biophys Acta. 2004; 1666:2–18. [PubMed: 15519305]
35. Hunte C, Richers S. Lipids and membrane protein structures. Curr Opin Struct Biol. 2008; 18:406–411. [PubMed: 18495472]
36. Govaerts C. Lipids Can Make Them Stick Together. Trends Biochem Sci. 2017; 42:329–330. [PubMed: 28363673]
37. Bai XC, et al. An atomic structure of human gamma-secretase. Nature. 2015; 525:212–217. [PubMed: 26280335]
38. Beatson S, Ponting CP. GIFT domains: linking eukaryotic intraflagellar transport and glycosylation to bacterial gliding. Trends Biochem Sci. 2004; 29:396–399. [PubMed: 15288869]
39. Bause E, Wesemann M, Bartoschek A, Breuer W. Epoxyethylglycyl peptides as inhibitors of oligosaccharyltransferase: double-labelling of the active site. Biochem J. 1997; 322(Pt 1):95–102. [PubMed: 9078248]
40. Chavan M, Rekowicz M, Lennarz W. Insight into functional aspects of Stt3p, a subunit of the oligosaccharyl transferase. Evidence for interaction of the N-terminal domain of Stt3p with the protein kinase C cascade. J Biol Chem. 2003; 278:51441–51447. [PubMed: 14530272]
41. Shrimal S, Cherepanova NA, Gilmore R. One flexible loop in OST lassos both substrates. Nat Struct Mol Biol. 2017; 24:1009–1010. [PubMed: 29215637]
42. Kern NR, et al. Lipid-linked oligosaccharides in membranes sample conformations that facilitate binding to oligosaccharyltransferase. Biophys J. 2014; 107:1885–1895. [PubMed: 25418169]
43. Harada Y, Li H, Li H, Lennarz WJ. Oligosaccharyltransferase directly binds to ribosome at a location near the translocon-binding site. Proc Natl Acad Sci U S A. 2009; 106:6945–6949. [PubMed: 19365066]
44. Shrimal S, Cherepanova NA, Gilmore R. DC2 and KCP2 mediate the interaction between the oligosaccharyltransferase and the ER translocon. J Cell Biol. 2017
45. Hakomori S. Glycosylation defining cancer malignancy: new wine in an old bottle. Proc Natl Acad Sci U S A. 2002; 99:10231–10233. [PubMed: 12149519]
46. Dube DH, Bertozzi CR. Glycans in cancer and inflammation--potential for therapeutics and diagnostics. Nat Rev Drug Discov. 2005; 4:477–488. [PubMed: 15931257]
47. Zheng SQ, et al. MotionCor2: anisotropic correction of beam-induced motion for improved cryo-electron microscopy. Nat Methods. 2017; 14:331–332. [PubMed: 28250466]
48. Zhang K. Gctf: Real-time CTF determination and correction. J Struct Biol. 2016; 193:1–12. [PubMed: 26592709]
49. Scheres SH. RELION: implementation of a Bayesian approach to cryo-EM structure determination. J Struct Biol. 2012; 180:519–530. [PubMed: 23000701]

50. Emsley P, Lohkamp B, Scott WG, Cowtan K. Features and development of Coot. Acta Crystallogr D Biol Crystallogr. 2010; 66:486–501. [PubMed: 20383002]

51. Pettersen EF, et al. UCSF Chimera--a visualization system for exploratory research and analysis. J Comput Chem. 2004; 25:1605–1612. [PubMed: 15264254]

52. Adams PD, et al. PHENIX: a comprehensive Python-based system for macromolecular structure solution. Acta Crystallogr D Biol Crystallogr. 2010; 66:213–221. [PubMed: 20124702]

53. Amunts A, et al. Structure of the yeast mitochondrial large ribosomal subunit. Science. 2014; 343:1485–1489. [PubMed: 24675956]

54. Chen VB, et al. MolProbity: all-atom structure validation for macromolecular crystallography. Acta Crystallogr D Biol Crystallogr. 2010; 66:12–21. [PubMed: 20057044]

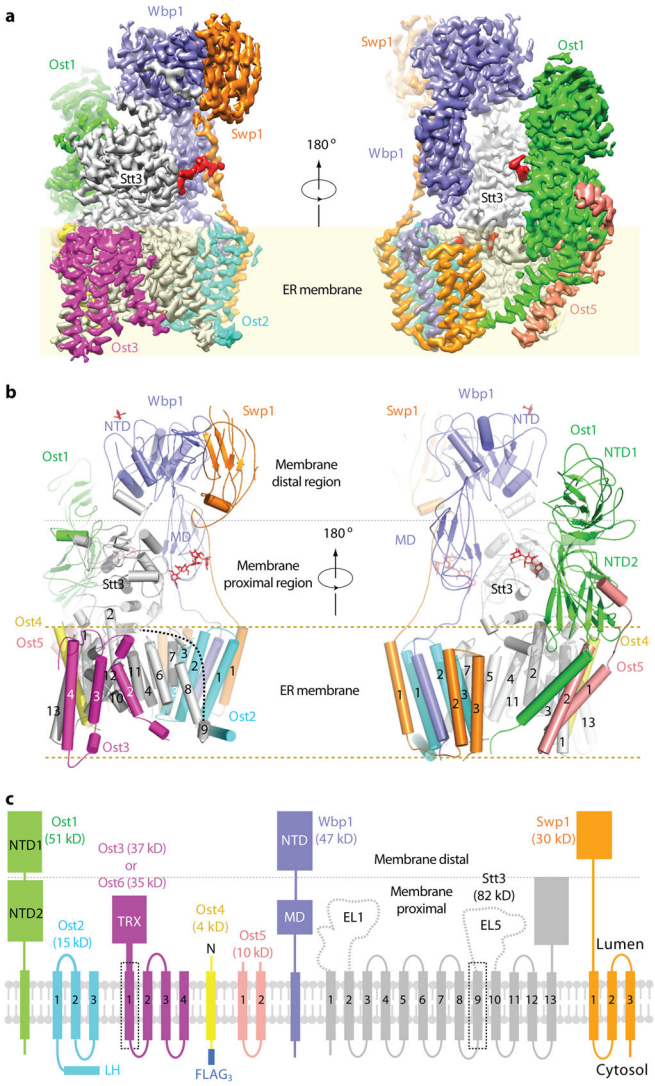

Figure 1. Subunit composition and atomic structure of the yeast OST complex

(**a**) Cryo-EM 3D map is shown in front and back views and colored by individual subunits. The shaded yellow rectangle represents the ER membrane. The three *N*-glycan densities are in red. (**b**) Atomic structure is shown in cartoons. Three *N*-linked glycans are displayed as sticks. The gray dotted line separates the membrane proximal- and membrane-distal lumenal regions. (**c**) The domain structures of the eight subunits. The letter N represents N-terminus of Ost4. EL1 and EL5 marks the external loops 1 and 5 in Stt3 transmembrane domain. Two flexible TMHs are highlighted with dotted squares.

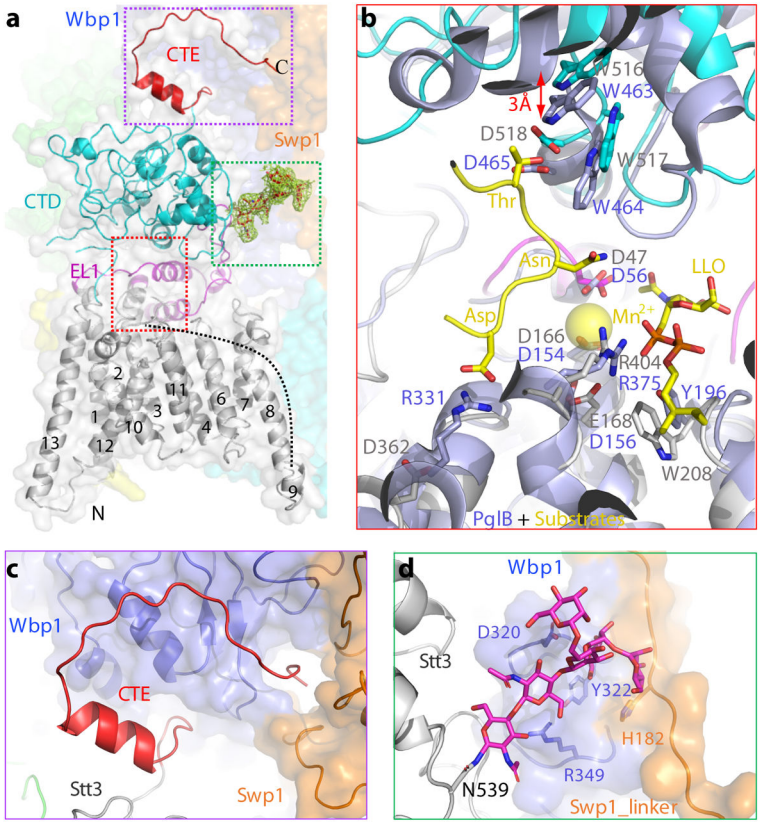

Figure 2. The atomic structure of Stt3

(a) Stt3 is shown as a cartoon. TMHs are in grey, CTD in cyan, EL1 in magenta, and CTE in red. The missing TMH9 is shown as a dotted black line. The green mesh is the *N*-glycan density of Asn539. The active site is highlighted by a dotted red square. The magenta dotted rectangle marks the Stt3 CTE interacting with Wbp1 and Swp1, and the green dotted square marks the *N*-glycan interacting with Wbp1 and Swp1. **(b–d)** are enlargements of the dotted boxes in **a**. The active site of Stt3 (**b**) is superimposed with the PglB structure (PDB ID 5OGL, light blue) in complex with Mn^{2+}, a peptide (DQNATF), and LLO analog ((ωZZZ)-PPC-GlcNAc in yellow sticks). The red arrow indicates an outward shift of Stt3 lumenal domain relative to that of PglB.

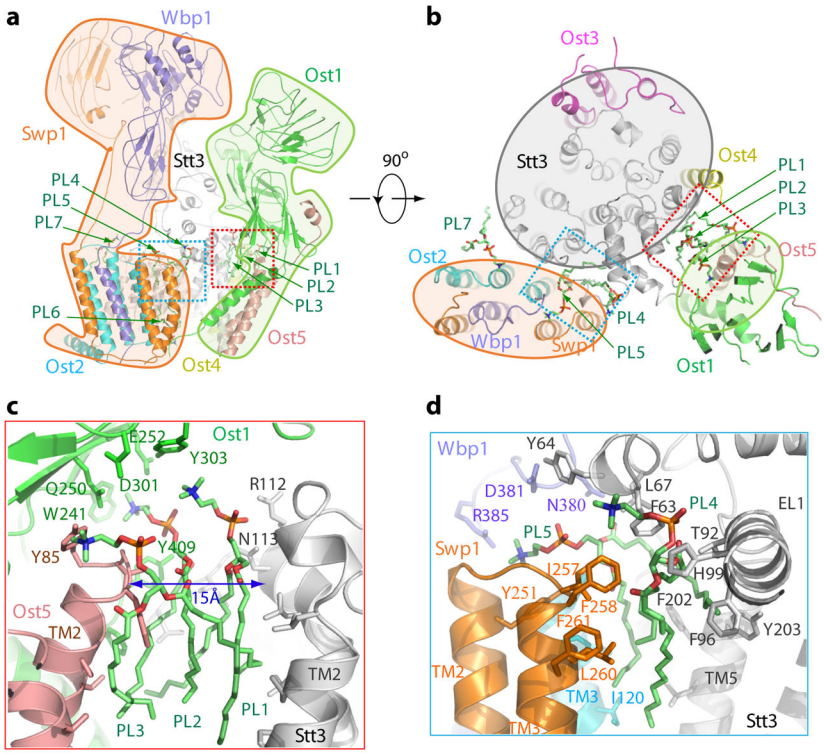

Figure 3. Assembly of the OST complex

OST is shown as cartoon in a side view (**a**) and a top (lumenal) view (**b**). Subcomplexes Ost1–Ost5, Ost2–Swp1–Wbp1, and Stt3–Ost3-Ost4 are highlighted by transparent shapes. The phospholipids PL1-7 are shown in green sticks. **(c)** Close-up view of the red box in **a** and **b**. PL1-3 mediate the interactions between Stt3 and Ost1–Ost5, filling a 15-Å gap at the interface. (**d**) Close-up view of the cyan box in **a** and **b**. PL4-6 mediate the interaction between Stt3 and Ost2–Swp1. PL6 in the lower leaflet of membrane is not visible here.

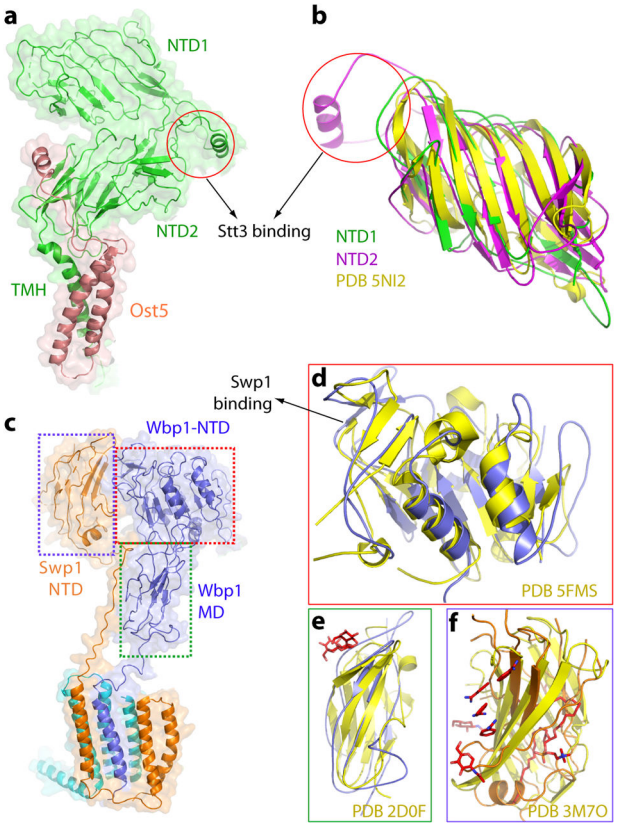

Figure 4. The atomic structures of the noncatalytic subunits

(a) Cartoon representation of subcomplex Ost1–Ost5. NTD1 and NTD2 of Ost1 are in green and magenta, respectively. Ost5 bridges Ost1 and Stt3. **(b)** Superposition of NTD1and NTD2 of Ost1 with the noncatalytic domain of human leukotriene A-4 aminopeptidase. **(c)** Cartoon representation of subcomplex Ost2–Wbp1–Swp1. The NTD and MD of Wbp1 and NTD of Swp1 are highlighted by three dotted squares. (**d)** Superposition of the NTD of Wbp1 (blue) and the NTD of GIFT52 (yellow). (**e)** Superposition of the MD of Wbp1 (blue) and the domain N of amylase (yellow). (**f)** Superposition of the Swp1 NTD (orange) and the MD-1 (yellow). The red sticks in **e** and **f** are substrates in the homolog crystal structures.

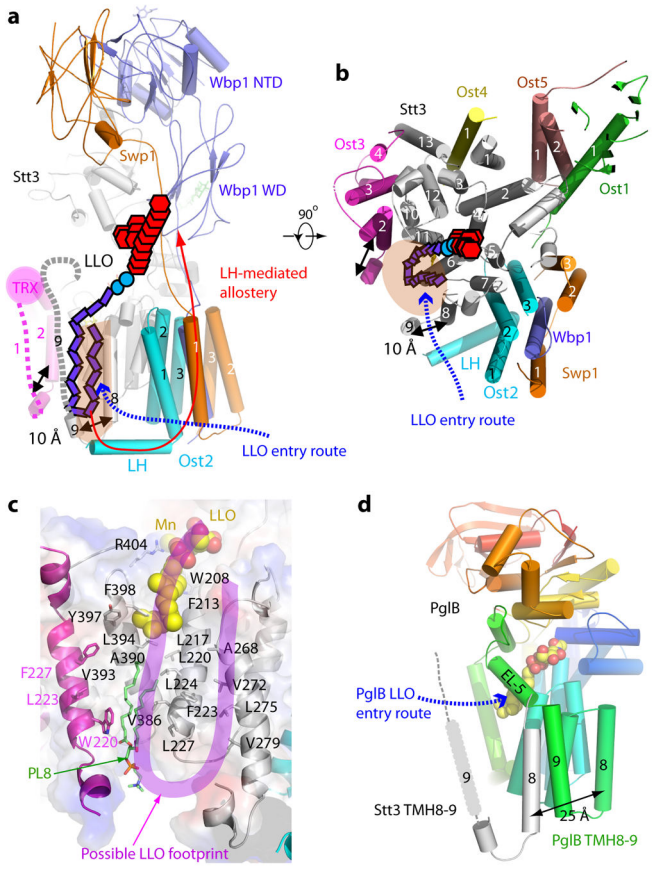

Figure 5. A possible LLO entry route and allosteric coupling by Ost2 LH

(a) The unresolved Stt3 TMH9 (gray dotted line) and Ost3 TMH1 (magenta dotted line) are 10 Å away from the central body of OST, forming an enlarge LLO-binding site. The gap between TMH8 and TMH9 of Stt3 is likely the LLO entry gate. The red curve indicates a likely path for allostery mediated by the Ost2 LH helix. The purple rectangles, cyan circles, and red hexagons represent dolichol, pyrophosphate, and OS, respectively. **(b)** The top (lumenal) view of the LLO-binding site. (**c**) The LLO-binding hydrophobic surface in OST. PL8 is the eighth phospholipid at the substrate binding surface. Mn^{2+} and the donor analog in PglB structure are superimposed and shown in yellow spheres. **(d)** Crystal structure of PglB (rainbow cartoon) in complex with LLO analog (yellow spheres). Stt3 TMHs8-9 (gray cartoon) are superimposed.

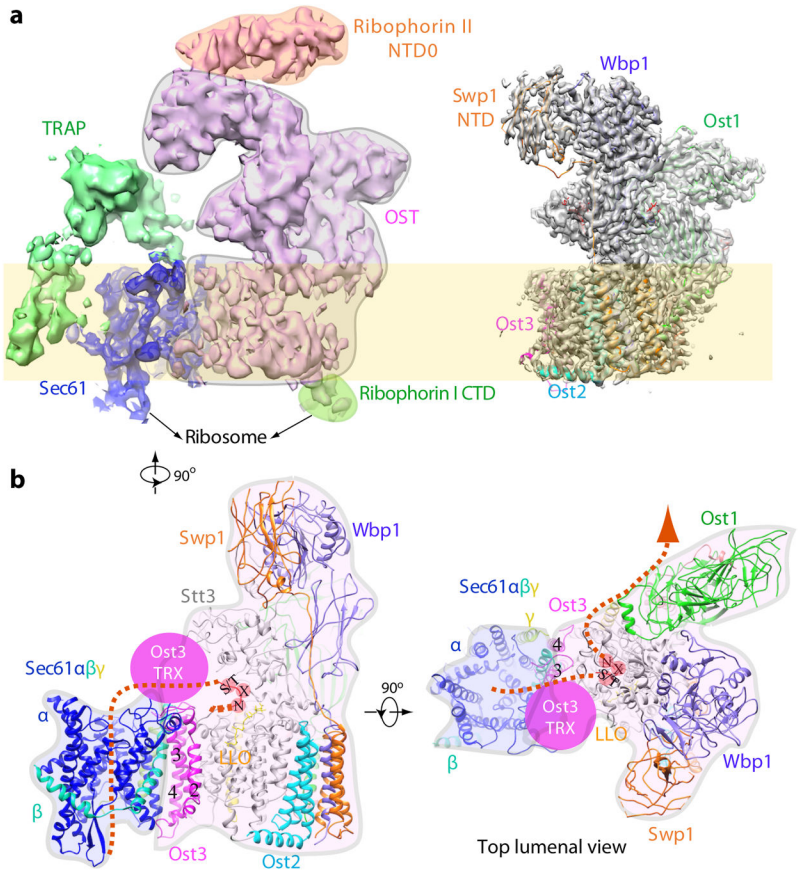

Figure 6. A model of the OST-translocon super-complex

(a) Comparison of the yeast OST 3D map (right panel) with cryo-ET map of a mammalian OST (purple), which is in complex with translocon (blue), TRAP (translocon-associated protein) complex (green), and ribosome (not shown) (EMD-3069). The mammalian OST has two extra domains: the cytosolic CTD in ribophorin I and lumenal NTD0 of ribophorin II. **(b)** A model of the OST-translocon super-complex, derived from docking OST structure and Sec61 structure (PDB ID: 3JC2). The dashed curve denotes the potential pathway for nascent peptide. See text for details.